

Synthetic control of the size, shape, and polydispersity of anisotropic silica colloids

Ryan P. Murphy,[†] Kunlun Hong,[‡] and Norman J. Wagner^{†}*

[†] Center for Molecular and Engineering Thermodynamics & Center for Neutron Science, Department of Chemical and Biomolecular Engineering, University of Delaware, Newark, Delaware 19716, United States

[‡] Center for Nanophase Materials Sciences, Oak Ridge National Laboratory, Oak Ridge, Tennessee 37831, United States

KEYWORDS: Nanoparticles, emulsions, anisotropic colloids, sol-gel, silica, rods

ABSTRACT

The microstructure and rheological properties of colloidal suspensions depend on particle size and shape. This work aims to further control the size, shape, and polydispersity of anisotropic silica colloids, to reduce particle size, and to provide additional mechanistic insights on a prevalent, water-in-oil emulsion synthesis method. Key findings show that the dimensions of anisotropic silica particles can be systematically varied by approximately five-fold, with a limiting minimum particle size ($D \approx 60$ nm, $L \approx 300$ nm) obtained from emulsions with excess polyvinylpyrrolidone (PVP) and sodium citrate. The synthesis conditions are identified and discussed for which the emulsion composition, temperature, sonication, polymer entanglements, mixing, and other perturbations may induce or mitigate emulsion instabilities, citrate precipitation, a competing mechanism of templated growth, termination of anisotropic growth, irregular silica structures, and fiber formation. An improved mechanistic understanding will expand the roadmap for rational design and synthetic control of anisotropic colloids using sol-gel silica chemistry confined within water-in-oil emulsions.

1. Introduction

Silica colloids are ubiquitous in many particle-based technologies designed for coatings, thermal and electrical insulators, fillers, drug delivery vehicles, and composite materials due to the unique properties of silica.[1] Rheological properties of silica-based suspensions such as the suspension viscosity, shear thinning, shear thickening, gelation behavior, and glass formation are intricately linked to the colloid size and shape.[2] Other characteristics such as the specific surface area, maximum packing fraction, diffusivity, sedimentation velocity, and liquid crystal behavior can also be tuned by controlling particle size and shape anisotropy.

A versatile strategy to synthesize anisotropic silica colloids with adjustable aspect ratios and shape features involves a water-in-oil emulsion method established previously.[3, 4] This adaptable colloidal system has opened exploration into the effects of particle shape anisotropy, for example, on the colloidal phase behavior,[5, 6] crystal transitions,[7, 8] and gelation behavior.[9] Additional synthetic efforts have also introduced unique shape adaptations,[10-16] multiple compositions,[10, 13, 16] thermoreversible attractions,[9] and fluorescent labelling of colloidal structures,[3, 17] all of which exist typically on micrometer length scales ($L \approx 1-4 \mu\text{m}$, $D \approx 300-500 \text{ nm}$). However, fewer studies have focused on routes to reduce the size of anisotropic silica particles toward sub-micrometer length scales with this emulsion method. Furthermore, the relatively large length polydispersity ($\approx 30-50\%$), prior to excessive washing and fractionation steps, has been largely ignored. Thus, there is motivation to further explore and build upon the standard emulsion-based method in order to control and reduce size dimensions by better understanding the mechanisms for initiation, propagation, and termination of anisotropic silica growth.

Previous studies have contributed an improved mechanistic understanding of the sol-gel growth of anisotropic silica colloids.[3, 4, 10, 18-22] In contrast to the synthesis of spherical silica colloids,[23] the hydrolysis and condensation of tetraethyl orthosilicate (TEOS) into non-spherical silica require anisotropic templates or an anisotropic supply of reagents to one side of a seed particle. Nakamura *et al.* and Miyaji *et al.* demonstrated routes to synthesize hollow rod-like silica particles, in which precipitated citrate or tartrate crystals served as templates for silica shell growth in ethanol-water-ammonia-salt mixtures.[18-20, 22] Work by Zhang *et al.* demonstrated a shape-selective and controllable method to produce rod-like silica colloids using a water-in-pentanol emulsion stabilized by citrate-coated gold nanoparticles and polyvinylpyrrolidone (PVP).[4] Their results initially suggested a soft-template growth process, in which a silica shell deposits onto a rod-like PVP-water-gold aggregate.[4] However, Kuijk *et al.* later demonstrated that the gold nanoparticles (stabilized by citrate) were not necessary to produce silica rods; rather, citrate was responsible for stabilizing aqueous droplets attached to the end of growing silica rods.[3] They demonstrated that rod growth initiates upon migration of a silica seed to the droplet interface, generating an anisotropic supply of hydrolyzed TEOS to one end of the rod.[3] The silica rod continues to grow predominantly along the length axis, with slower growth along the radial axis, until the depletion of TEOS or the destabilization of the liquid-liquid-solid droplet interface.[3] Citrate and PVP are both necessary to stabilize anisotropic growth using this emulsion method [3, 10], but their specific interactions and roles are not entirely understood and warrant further investigation.

As examples of how variations in synthetic conditions can yield significant changes in particle morphology, a study by Datskos and Sharma showed that varying temperature could produce silica rods with segmented ridges and with a reduced diameter at higher temperatures ($D \approx 150$ nm at

65 °C).[14] In a separate study, they also observed multimodal distributions of long, thin silica fibers ($D \approx 20\text{-}65$ nm, $L \approx 30\text{-}100$ μm) by applying bath sonication during the reaction.[24] Anisotropic silica colloids with reduced dimensions may benefit certain applications that desire higher specific surface area, low particle volume fraction, limited effects of sedimentation, and access to regimes with low Péclet number for rheological investigations.

In this work, the combined effects of emulsion composition, temperature, and sonication are further explored with the aim to better control and, in particular, reduce the size of anisotropic silica colloids. We demonstrate that approximately five-fold reductions in rod dimensions ($D \approx 60$ nm, $L \approx 300$ nm) are best achievable by systematically adjusting the emulsion composition. It is also demonstrated that long, thin silica fibers can be produced by addition of excess sodium citrate without sonication, leading to the proposition that such fibers arise from a competing mechanism of templated growth due to emulsion instabilities and citrate precipitation. This study provides additional mechanistic insight on the role of stabilizing reagents, polyvinylpyrrolidone (PVP) and sodium citrate, which together strongly influence silica growth, particle dimensions, end shape, and overall shape anisotropy. Results and discussions are divided into five sections that focus on the effects of (3.1) temperature, (3.2) sonication, (3.3) citrate precipitation, (3.4) emulsion composition, and (3.5) scale-up.

2. Experimental

2.1 Particle synthesis. Anisotropic silica colloids were synthesized based on previously established protocols,[3, 9] in which a silica precursor (tetraethyl orthosilicate, TEOS, ACROS Organics, 98%) is injected into an emulsion containing 1-pentanol (ACROS Organics, 99%),

polyvinylpyrrolidone (PVP, 3.5 kDa, 40 kDa, or 1300 kDa, ACROS Organics and Sigma Aldrich, 95%), ethanol (Decon Labs, 200 proof), water (18.2 M Ω -cm), ammonia (Merck, 25 wt% aq.), and sodium citrate (trisodium citrate dihydrate, disodium citrate sesquihydrate, or monosodium citrate, Fisher Scientific, 99%). All reagents were used as received without further purification.

For the standard small-scale reaction, 1 g of PVP (40 kDa) was added to 10 mL of pentanol in a 20 mL glass scintillation vial and was distributed by vortex mixing (3000 rpm). 1 mL of ethanol and 0.28 mL of water were added, and the mixture was vortexed for 1 min. Then, 0.1 mL of 0.18 M aqueous trisodium citrate dihydrate (citrate) was injected and quickly distributed by vortex mixing for 1 min, followed by the addition of 0.2 mL of ammonia (25 wt% aq.) with vortex mixing for 1 min. Lastly, 0.1 mL of TEOS was injected and quickly vortexed for 10 s. All mixtures reacted without stirring at room temperature overnight for 18-24 hours or as listed in the Supporting Information, Table S1. For large-scale reactions, the reagents were scaled up approximately 30-fold and mixed in a 1 L HDPE bottle, as listed in the Supporting Information, Table S1. Emulsions with high PVP concentration or molecular weight (34-51 wt% PVP or 1300 kDa) were heated to 40 °C and shaken frequently to assist PVP dissolution into pentanol, ethanol, and water, and then were cooled to room temperature prior to adding citrate, ammonia, and TEOS.

Adaptations to these standard conditions included single or combined variations in (1) temperature from 4, 20, 40, 60, and 80 °C; (2) bath sonication power from 57, 185, and 470 W at 40 kHz; (3) PVP molecular weight from 3.5, 40, and 1300 kDa; (4) PVP concentration from 9-51 wt%; (5) sodium citrate salts with mono-, di-, and tri-sodium counter ions; (6) citrate concentration from 0.04-1.5 wt%; (7) water concentration from 2.5-5 wt%; and (8) ethanol

concentration from 0.0-7.5 wt%. The specific reaction conditions and reagent additions are tabulated in the Supporting Information, Table S1.

For reactions at higher temperatures (40, 60, 80 °C, ± 1 °C), the emulsion was heated to the desired temperature prior to TEOS injection using a water bath or electrical heating block. After equilibrating the emulsion at the desired temperature for 15 min, TEOS was injected into the mixture and immediately vortex mixed for 10 s. The reaction proceeded without stirring for 0.5-4 h at 40 or 60 °C, and for 0.25-1 h at 80 °C. Reactions were quenched by dilution in cold ethanol.

For reactions that employed bath sonication, samples were positioned in a water bath sonicator immediately following TEOS injection. The bath sonicator power input was varied from 57 W, 185 W, and 470 W at fixed 40 kHz. For consistency, reaction vials were positioned in approximately the same center position of the bath sonicator to limit possible effects of uneven power intensity distribution within the bath sonicator. Water was exchanged to heat or cool the sonication bath to maintain temperatures at 4 °C, 20 °C, and 40 °C with temperature fluctuations ± 5 °C.

After the reaction, the mixtures were poured into ~20 mL of cold ethanol within a 50 mL conical centrifuge tube and centrifuged at 6000 g for 60 min, after which the supernatant was decanted and discarded. The sediment was resuspended in ethanol with vortex mixing and bath sonication, washed, and centrifuged twice more in ethanol (6000 g, 30 min). Then, the sediment was washed and centrifugation twice in water (6000 g, 30 min). After the last water wash, the sediment was suspended in ethanol by vortex mixing and sonication. So as to examine entire particle size populations, particles were not fractionated by additional centrifugation steps. However, large-

scale reactions received additional fractionation steps to improve size polydispersity by centrifuging in ethanol an additional three times (700 g, 15 min), discarding the supernatant after each centrifugation, and a final centrifugation step was performed (100 g, 5 min) to remove large rods or aggregates by discarding the sediment.

2.2 Scanning and transmission electron microscopy (SEM, TEM). Silica particles were imaged with a Zeiss Merlin SEM operating at 1 kV at 100 pA. Samples were made by pipetting 3 μL of sample (~ 0.5 wt% silica particles suspended in ethanol) onto a cleaned silicon wafer and dried in air. The particle dimensions of randomly selected particles were measured and analyzed with ImageJ software to obtain the number average mid-point diameter and standard deviation (D , σ_D), the number average end-to-end length and standard deviation (L , σ_L), and the apparent aspect ratio and standard deviation ($AR=L/D$, σ_{AR}) for 30-60 particles per sample.

Select samples were imaged by TEM using an FEI Tecnai G2 Twin instrument operating at 120 kV and 3 μA . Images were captured using a Gatan CCD camera. Samples were prepared by pipetting 3 μL of sample in ethanol onto a Formvar/carbon-coated copper grid (200 mesh) and dried in air.

2.3 Ultra-small angle X-ray scattering (USAXS): USAXS experiments were performed on the 9-ID-C beamline at the Advanced Photon Source at Argonne National Laboratory. The slit-smear scattered intensity was collected over a q -range of $0.0001 \text{ \AA}^{-1} < q < 1 \text{ \AA}^{-1}$, in which q is the scattering wave vector $q = 4\pi\lambda^{-1}\sin(\theta/2)$, θ is the scattering angle, and λ is the incident X-ray wavelength (0.689 \AA , 18 keV). Samples were suspended and diluted in ethanol (5 mg/mL), loaded in glass capillaries (KIMAX, 1.5-1.8 OD), and sealed with wax to limit solvent evaporation.

The empty glass capillary scattering was subtracted from the sample scattering using the standard reduction procedures provided with the Indra, Irena, and Nika software packages.[25-27] Scattering data were fit with a polydisperse cylinder form factor model with a Schulz distribution in length and radius using the SasView software package v3.1.2.[28, 29] Model fit parameters are listed in the Supporting Information, Table S3.

3. Results and discussion

SEM images (Fig. 1) show the anisotropic particles generally exhibit a truncated spherocylinder geometry, which is a consequence of the “standard growth” mechanism of TEOS hydrolysis and condensation occurring within an end-attached aqueous droplet.[3] The characteristic particle length (L) is defined as the number average end-to-end length, and the particle diameter (D) is defined as the number average diameter at the midpoint (to average tapering effects). We focus our efforts and discussions on routes to decrease the particle diameter D , since tuning the silica precursor concentration (tetraethyl orthosilicate, TEOS) or reaction time linearly correlates with particle length L . [3, 10] Furthermore, increasing both D and L can be more easily achieved by seeding and subsequent TEOS coating steps.[3]

SEM images in Fig. 1 show the rich diversity in particle sizes and shapes obtained from different emulsion conditions. The washed, unfractionated silica particles serve as fossils of the sol-gel reaction within the emulsion, wherein specific features of the individual particles (D , L , branching, curvature, end effects, hollow cavities) and the particle size distributions provide clues for the mechanisms of anisotropic growth and termination. As a reference for comparison, “standard rods” refer to the unfractionated rods using the standard conditions (Fig. 1m,

$D \approx 260$ nm, $L \approx 1900$ nm). Figure 2 quantifies the average particle D , L , and sample standard deviations (error bars) to map the general trends conveyed qualitatively in Fig. 1. Detailed synthesis conditions and particle dimensions from SEM are tabulated in the Supporting Information, Table S1 and S2, respectively. The symbol colors and shaded regions correspond to classification groups shown in Figs. 1 and 2, as defined in the caption and also in Table S1 and Table S2.

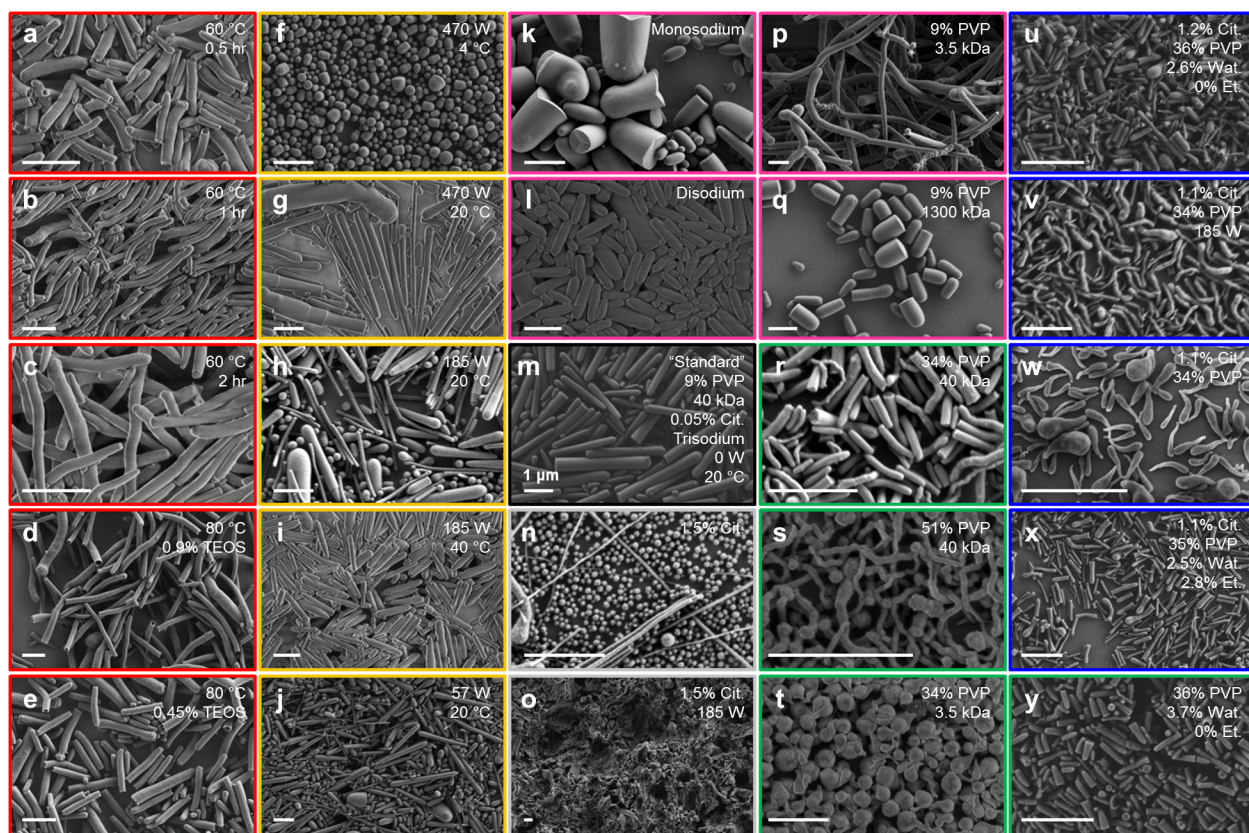


Figure 1. SEM images of anisotropic silica particles from various adaptations to the (m, black) standard conditions. The image outline color corresponds to key changes in (a-e, red) temperature, TEOS wt%, and reaction time; (f-j, orange) sonication power input and temperature; (k, l, p, q, pink) sodium counter ion concentration or PVP molecular weight; (n, o, gray) sodium citrate wt%; (r, s, t, y, green) PVP wt% and molecular weight; (u-x, blue) combined excess PVP

and citrate wt%; and (u, x, y) further variations in ethanol and water wt%. Text in the upper right corner highlights the main deviations from the standard method. The scale bar is 1 μm for all images.

3.1. Temperature. Increasing the reaction temperature to 60 $^{\circ}\text{C}$ or 80 $^{\circ}\text{C}$ was found to decrease the diameter of the silica rods to $D \approx 150\text{-}200$ nm. In general, the particle length could be increased (decreased) by increasing (decreasing) the reaction time (Fig. 1a-c) or TEOS concentration (Fig. 1d-e). This reduction in diameter was consistent with previous results,[14] suggesting a fundamental limit to reducing $D \approx 150$ nm at temperatures up to 80 $^{\circ}\text{C}$. Additional effects of increasing the temperature also induced curved, branched, and hollow-ended structures (see also SI Fig. S1). The particle curvature and branching were thought to occur from the enhanced Brownian motion of rods and terminal aqueous droplets, as well as a greater probability for collision and coalescence of neighboring droplets. The hollow-ended structures that occur at elevated temperatures are likely due to the faster rate of TEOS hydrolysis and condensation relative to the diffusion within the terminal aqueous droplet, which was consistent with previous observations of hollow silica structures produced by increasing the ammonia (catalyst) concentration.[30] The possible advantage of these curved and branched silica structures remains unknown, but the enhanced mass transport, reduced viscosity, and lower reaction time achieved with higher temperatures (40-80 $^{\circ}\text{C}$) could significantly benefit reaction scale-up, processing, and separations from an industrial perspective.

3.2 Sonication. An alternative strategy to further reduce rod diameter focused on using bath sonication, which was employed throughout select reactions with varying input power (fixed 40 kHz) and temperature (Fig. 1f-j). Applying bath sonication (Fig. 1h, 185 W, 7 h) produced a multimodal mixture of thin rods or fibers ($D \approx 30\text{-}100$ nm), larger rods of varying lengths

($D \approx 250$ nm), and spheres ($D \approx 200$ - 250 nm). Surprisingly, the production of thin rods appeared to be suppressed by increasing the sonication power input (Fig 1g, 470 W) or by sonicating at higher temperatures (Fig. 1i, 185 W, 40 °C). Furthermore, increasing sonication power input at low temperatures produced silica particles with modest shape anisotropy, and no thin silica rods or fibers (Fig 1f, 470 W, 4 °C).

Together, these observations suggested the role of sonication mainly acted to destabilize the terminal-water droplet during standard rod growth, resulting in the occasional formation of thin rods or fibers. The larger size dispersities and multimodal distributions could not be readily controlled by adjusting sonication power or temperature to favor production of these thin silica rods. Despite this poor control, these results were significant by demonstrating (1) the formation of thin silica rods is possible, (2) the underlying mechanism for growth of thin silica rods and fibers competes with the standard rod growth mechanism, and (3) different conditions can be adjusted, to some degree, to favor or hinder competing growth mechanisms.

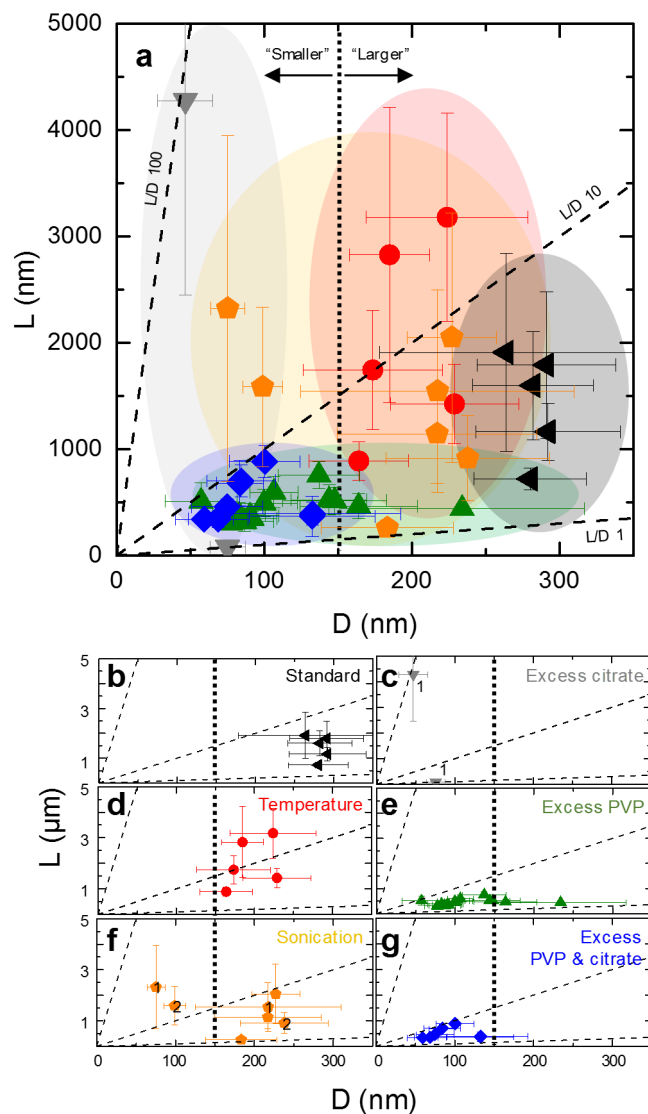


Figure 2. (a) Map of particle size depending on synthesis conditions: (b) standard conditions, (c) excess citrate (d) temperature, (e) excess PVP, (f) sonication, (g) combined excess PVP and citrate. The average end-to-end length (L), diameter (D), and standard deviations (error bars) are quantified and grouped, in which symbol colors and shaded regions correspond to images in Fig. 1 and the Supporting Information, Table S1 and S2. Multimodal distributions are indicated by the superscripts next to symbols in (c) and (f).

3.3 Citrate precipitation. How are these thin silica rods ($D < 100$ nm) produced as a result of sonication? Based on previous observations of templated silica growth onto citrate templates without pentanol or PVP,[31] it was hypothesized that nucleation and growth of anisotropic precipitates or crystals of citrate could likewise serve as templates for silica growth to form thinner silica rods when confined within a pentanol emulsion. If the rate of precipitation is significant, it could disrupt or compete with the standard rod growth mechanism. We speculate that this citrate precipitation could occur spontaneously without mechanical perturbation, given sufficient time, due to the inherent insolubility of citrate in the primary components of the non-aqueous phase, pentanol (77 wt%) and ethanol (7.5 wt%). Perturbations to the emulsion that arise from shear fields, vibrations, or sound waves could increase the rate of precipitation by enhancing mass transport, by rupturing the water-oil emulsion interface, by generating thermal or concentration gradients, or by enhancing fluctuations in the localized citrate concentration, wherein the latter mechanisms accelerate nucleation. Conversely, adding reagents with an affinity for citrate in the aqueous phase, in this case water (5 wt%) or PVP (9 wt%), could decrease the rate of precipitation or eliminate phase separation altogether. However, given the complexity of this system, the overall effect of such perturbations likely changes as a function of time throughout the sol-gel reaction. For example, the propensity for citrate precipitation could increase throughout the conversion of TEOS to silica by locally producing ethanol (poor solvent) and consuming water (good solvent). Ultimately, a competition of templated growth and standard rod growth could explain the presence of multimodal populations of thin rods, fibers, spheres, and standard rods.

To further test this hypothesis, an emulsion with significant excess of sodium citrate (1.5 wt%) was allowed to react without sonication or stirring throughout the reaction. As shown in Fig. 3a,

the emulsion mixture is significantly more turbid than standard conditions, which is indicative of phase separation or precipitation. In addition to producing visible precipitates, the reaction with excess citrate also produced a mixture of thin silica fibers, thin rods, standard rods, and primarily small spheres (Fig. 1n, $D \approx 75$ nm, see also SI Fig. S2). These smaller silica spheres could be nucleates from citrate precipitates that failed to grow into longer rods or fibers. If the same mixture containing excess citrate is sonicated during the reaction, only very large precipitates and irregular structures are formed instead (Fig. 1o).

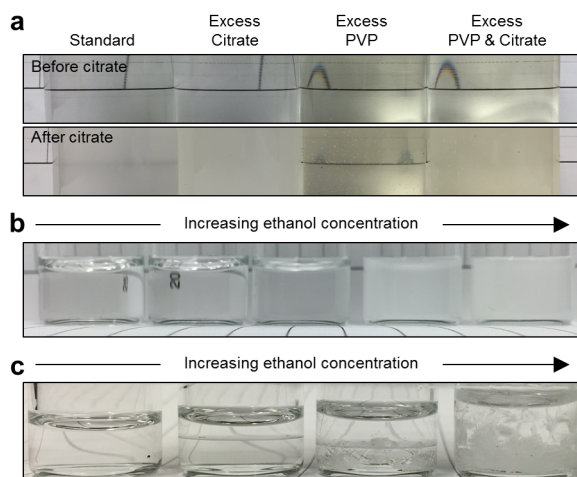


Figure 3. (a) Qualitative changes in the emulsion turbidity shown for (top) before citrate addition and (bottom) after citrate addition. Left to right shows the standard emulsion (9 wt% PVP, 0.05 wt% citrate), with excess citrate (9 wt% PVP, 1.5 wt% citrate), excess PVP (34 wt% PVP, 0.04 wt% citrate), and excess PVP and citrate (34 wt% PVP, 1.1 wt% citrate). (b) Water-ethanol-citrate mixtures with 0.6 wt% citrate show increasing turbidity due to precipitation of sodium citrate for mixtures containing (left to right) at 50%, 60%, 70%, 80%, and 90 vol% ethanol. (c) Partitioning and phase separation occurs at higher concentrations of sodium citrate (left to right) with 26%, 23%, 21%, 18 wt% citrate in a water-ethanol-citrate

mixture with 17%, 29%, 38%, and 50 vol% ethanol. Initially, a liquid-liquid boundary between the citrate-rich phase (bottom) and the citrate-poor phase (top) forms, followed by nucleation and growth of rod-like citrate crystals from the metastable citrate-rich phase.

The competition between these two growth mechanisms, namely templated growth and the standard terminal-droplet growth, offers one explanation for the multimodal distributions obtained after sonication, stirring, or excess citrate is introduced. Furthermore, the formation of thin silica fibers and rods *without* sonication suggests that previous observations[24] of hollow silica fibers during bath sonication ($D \approx 30$ nm, $L \approx 100$ μ m) could be explained by nucleation and growth of long citrate fibers, which subsequently act as water-soluble templates for PVP adsorption and growth of a porous silica shell.[32] Our results agree with the previous observations by Datskos and Sharma,[24] but provide additional evidence against the hypothesized, alternative mechanisms of a cavitation-induced or the fiber-spinning mechanism during sonication. Instead, our results support the hypothesis of emulsion destabilization, which is reasoned to be from sonication-induced citrate precipitation. Other relevant observations of smaller, irregular silica particles produced by stirring were also speculated to occur from destabilization of the terminal aqueous droplet and precipitate formation.[3]

A simplified demonstration for citrate precipitation in water-ethanol mixtures (Fig. 3b, 0.6 wt% citrate) shows that increasing the ethanol concentration eventually results in a turbid mixture (near ≈ 70 vol% ethanol) – a signature of precipitate formation. Binodal phase boundaries for pentanol-water-citrate or ethanol-water-citrate also indicate that at higher citrate concentrations (>2 wt%), increasing pentanol concentration leads to L-L phase separation, and increasing ethanol concentration leads to S-L separation (precipitation).[33, 34] Figure 3c shows layered liquid-

liquid phase separation and subsequent crystallization at very high citrate concentrations (18-26 wt% citrate) and lower ethanol concentrations (17-50 vol% ethanol in water), in which macroscopic rod-like crystals nucleate and grow from the citrate-rich layer at different rates depending on the ethanol concentration. It should be cautioned that important factors are neglected in this simplified example system, such as the emulsion components (pentanol, PVP, and ammonia), interfacial energy, and surface forces present between the aqueous droplets and surrounding pentanol matrix. Nevertheless, the distinct changes in turbidity for the full emulsion shown in Fig. 3a hint that delayed phase separation or precipitation of citrate can occur, to some extent, which may influence the growth of silica rods.

The templated growth of hollow silica rods and fibers onto tartrate or citrate crystals have been reported previously for a similar reaction mixture without pentanol (i.e., ethanol, water, citrate or racemic *dl*-tartrate, ammonia, and TEOS).[18, 19, 22, 31] Hollow silica tubes that formed in these mixtures typically exhibited larger and broader particle length scales ($D \approx 0.05\text{-}1\ \mu\text{m}$, $L \approx 0.5\text{-}300\ \mu\text{m}$)[18, 19, 22] than those reported with the pentanol emulsion method. These differences likely stem from reagent partitioning and reaction confinement within the 100-300 nm aqueous droplets in pentanol.

The propensity for citrate precipitation also offers one explanation for the observed tapering effects and tailing effects for some particles (Fig. 4a, see also SI Fig. S3), which have been reported elsewhere.[3, 6, 9] During rod tapering or tailing, the diameter decreases slowly or abruptly to a short rounded point or long tail at the end, respectively, which is in contrast to the flat-end anticipated for the ideal standard terminal-droplet growth mechanism. Surprisingly similar observations of tapering effects were reported for an ethanol-water reaction mixture (without droplet confinement within a pentanol phase), in which square-shaped hollow cavities within silica

tubes reportedly decreased gradually in diameter from one end to the other.[20] A following study claimed that evidence of X-ray powder diffraction peaks for *unwashed* samples strongly supported a crystal template growth mechanism, in which needle-like crystals (ammonium *dl*-tartrate or ammonium oxalate) acted as templates for porous, amorphous silica shell growth.[22] Typical water washing steps during workup and purification should dissolve and remove water-soluble crystal templates, thus creating a hollow core-shell silica structure, only if the surrounding silica shell forms a penetrable tube or porous structure that aids diffusion. Further understanding of this mechanism for undesirable droplet destabilization and subsequent termination of anisotropic growth via citrate precipitation may help reduce rod length polydispersity and thereby improve yields by reducing the need for substantial particle fractionation steps.[3, 6, 9]

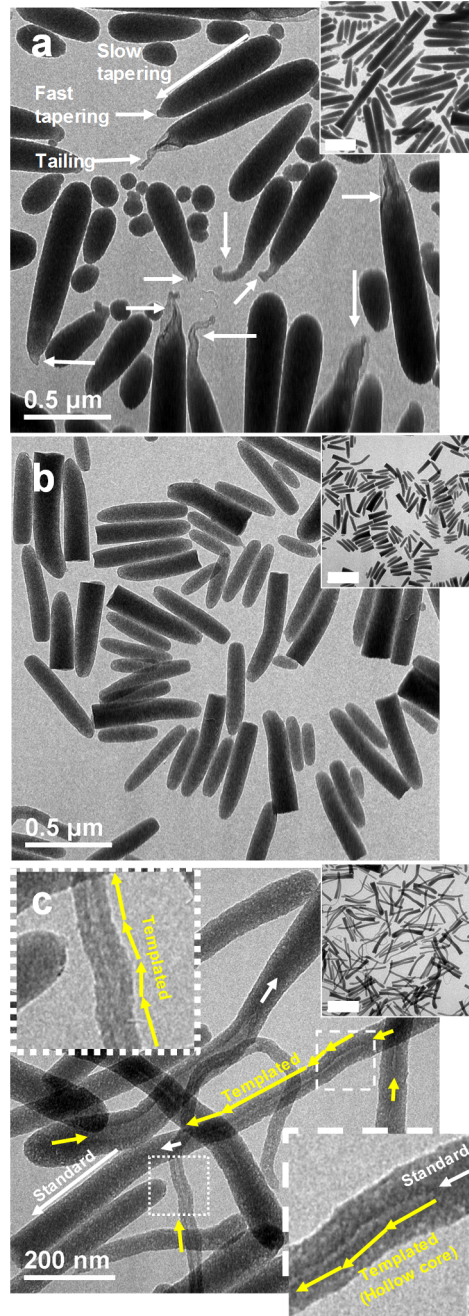


Figure 4. TEM images showing tapering, tailing, and hollow core-shell silica structures for washed and unfractionated samples from different emulsion conditions (a) standard, (b) excess PVP and (c) combined excess PVP and citrate. (a) Compared to longer silica rods that have a flat end, shorter silica rods produced during standard emulsion conditions generally exhibited a slowly tapering diameter, a pointed end (fast tapering), or a long tail-like structure (tailing) as indicated

by the white arrows. (b) Tailing effects and length polydispersity were qualitatively reduced for emulsions with excess PVP (34 wt%, 40 kDa), in addition to reducing the overall rod dimensions. (c) Emulsions with excess PVP and excess citrate (34 wt% PVP, 40 kDa, 1.1 wt% citrate) showed silica rods with occasional hollow core-shell sections along the length of the rod, which coincided with curvature of the rod. Inset regions (dotted and dashed boxes) show that the hollow core region from templated growth can initiate (yellow arrows) and resort back to standard rod growth (white arrows), suggesting competition between these two growth mechanisms. Scale bars in the upper right inset images are 1 μm .

Although the standard citrate salt typically comprises only ≈ 0.05 wt% of the emulsion, the resulting particle dimensions, size distributions, overall shape, and end-effects are highly sensitive to citrate concentration and sodium counter ions. Figure 1k-l demonstrated this sensitivity by showing diameters that range from ≈ 200 nm (disodium) up to ≈ 500 nm (monosodium) with equivalent citrate ion concentrations (≈ 0.01 mol% citrate ions). Intriguing v-shaped ends were also observed from emulsions with monosodium citrate at equivalent citrate ion concentrations (Fig. 1k), as well as for higher concentrations of trisodium citrate and PVP (see SI Fig. S4). It is unclear how these irregular ends form, but it may occur from preferential growth along facets of citrate crystals or precipitates confined within the aqueous terminal-droplets.[31]

The presumed primary role of citrate acts to stabilize the aqueous droplet interface. Here it is indicated that citrate can also act as a template for growth of hollow silica nanotubes, which competes with the standard terminal-droplet growth and can terminate anisotropic growth altogether by destabilizing the terminal droplet. As shown for similar ethanol-water-ammonia-salt

mixtures,[18, 19, 22] different organic salts may further improve the control of the particle size, shape, polydispersity, and particle porosity when confined within the pentanol-water emulsion.

3.4 Emulsion composition. Variations to the standard emulsion composition were explored by focusing on the stabilizing agents, PVP and citrate. First, addition of high molecular weight PVP (Fig. 1q, 1300 kDa, 9 wt% PVP) produced low aspect ratio rods ($L/D < 3$), while addition of low molecular weight PVP (Fig. 1p, 3.5 kDa, 9 wt% PVP) caused phase separation and production of worm-like structures, small clusters, and spheres (see also SI Fig. S5).

Second, a decrease in silica rod dimensions ($D \approx 100$ nm, $L \approx 600$ nm) was achieved by the addition of excess PVP at the standard molecular weight (Fig. 1r and Fig. 4b,

34 wt% PVP, 40 kDa). Further increasing the PVP concentration produced highly curved,

worm-like silica particles with $D \approx 60$ nm (Fig. 1s, 40 kDa, 51 wt% PVP). However, this

51 wt% PVP emulsion had an impractically high viscosity and low silica yield. To reduce the emulsion viscosity, a lower molecular weight PVP (3.5 kDa) was added at 34 wt% PVP.

Interestingly, emulsions with excess PVP 3.5 kDa did not phase separate, as observed for lower concentrations (Fig. 1p), but rather, produced short-tailed structures (Fig. 1t, 34 wt% PVP,

3.5 kDa). Together, this dependence of silica growth on PVP molecular weight and

concentration suggests that the initial emulsion droplet size, terminal droplet stability, and

subsequent growth of anisotropic silica structures may fundamentally depend on the number of

polymer entanglements. For the emulsions containing PVP 3.5 kDa, which was below the entanglement molecular weight (estimated PVP $M_e = 16.8$ kDa),[35] no straight rods were

observed, even at higher PVP concentrations (see SI Fig. S6 at 51 wt%). Based on previous

observations that indicate a high concentration of PVP exists within the aqueous droplets [3, 10],

it is speculated that polymer entanglements improve the elasticity, adsorption, and steric stability

of the terminal droplet to balance against competing forces that can destabilize the droplet, which terminates anisotropic growth. TEM results in Figure 4b showed that the length polydispersity could be improved and the tailing effects could be mitigated with excess PVP (34 wt% PVP, 40 kDa) when above the entanglement molecular weight. However, conditions with excess PVP also induced some curvature, which may be from the confinement of silica rods growing within a crowded, viscous emulsion. Mitigation of citrate precipitation by addition of excess PVP was also qualitatively indicated by the lower emulsion turbidity shown in Fig. 3a.

Lastly, a further decrease in the silica rod diameter to $D \approx 60\text{-}100$ nm was achieved by combining the diameter-reducing effects of excess citrate and excess PVP, as shown in Fig. 1u-x, Fig. 2g, and Fig. 5. Adding both excess citrate (≈ 1.1 wt%) and excess PVP (34 wt%, 40 kDa) consistently reduced the particle diameter, presumably by shrinking the emulsion droplet while mitigating citrate precipitation and longer fiber formation. Similarly high concentrations of citrate showed significant precipitation and fiber formation with lower PVP content (Fig. 1n and SI Fig. S2, 1.5 wt% citrate, 9 wt% PVP), but it appeared that excess PVP constrained the precipitation such that no long fibers were observed. In addition to reducing the particle diameter, a closer examination using TEM (Fig. 4c) revealed formation of hollow core-shell regions, segments with enhanced curvature, and peculiar v-shaped end effects (see also SI Fig. S4). These hollow core-shell structures suggested that templated growth was more favorable and controllable at high PVP and citrate concentrations. Furthermore, Fig. 4c confirmed the competition and toggling between a standard growth mechanism (white arrows) and a templated growth mechanism (yellow arrows), in which distinct regions along the silica rod exhibited a filled core or hollow core, respectively. This hollow core-shell structure was analogous to the templating of a porous silica shell onto citrate precipitates or crystals, as

previously observed in water-ethanol-ammonia-salt mixtures without confinement within pentanol.[18-20, 22, 31] A greater degree of curvature and narrowing of the diameter within the (hollow) templated regions suggested that templated growth occurred sporadically and at a faster rate along the length axis, as compared to (non-hollow) rod-like segments produced from standard terminal-droplet growth. Additional variations in water and ethanol concentrations influenced the particle curvature and polydispersity, but overall produced less significant changes to D (Fig. 2g), which suggested a fundamental lower limit to $D \approx 50\text{-}60$ nm under these conditions of excess PVP and citrate. Further adjustments and optimization to the emulsion conditions, such as by tuning the ammonium ion concentration and PVP molecular weight, are necessary to produce more idealized “straight” rods with less curvature, lower length polydispersity, and reduced diameter.

3.5 Scale-up. Consistent trends for reducing rod diameter with excess PVP and citrate were confirmed after scaling up the reaction volume by thirty-fold. Figure 5 shows ultra-small angle X-ray scattering (USAXS) data obtained at the Advanced Photon Source on beamline 9-ID-C.[25-27] The scattering data were fit using a polydisperse cylinder form factor model, with parameters listed in SI Table S3.[9, 28, 29] The shift of scattered intensity to higher q (scattering vector) and the corresponding model fits showed a decrease in D from the standard conditions (red circles, $D \approx 290$ nm), excess PVP (green squares, $D \approx 140$ nm), and excess PVP and citrate (blue triangles, $D \approx 90$ nm). Coincident with this reduction in diameter, the polydispersity ratio (σ_D/D_{mean}) along the radial axis increased from 0.19 (red), 0.29 (green), 0.42 (blue), which was a consistent trend for USAXS and SEM size analysis that showed $\sigma_D \approx 40\text{-}60$ nm. Previous studies have found that scaling up the reaction volume can change the apparent average length and diameter.[3, 9] These trends are thought to occur from inconsistent mixing methods and the

specific mixing energy input. Given the strong sensitivity of the particle size and shape to the citrate concentration, imposing different mixing methods, shear rates, and mixing timescales may influence the rate and extent of citrate precipitation within the emulsion, thereby producing inconsistencies in aqueous droplet composition and average droplet diameters upon initiation.

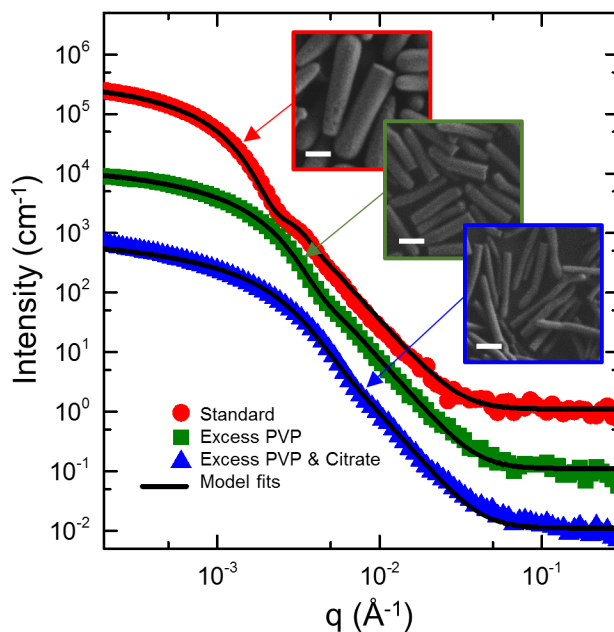


Figure 5. Ultra-small angle X-ray scattering of silica rods produced from scaled-up reactions with (G2, red circles) standard conditions, (E14, green squares) excess PVP, and (F7, blue triangles) excess PVP and citrate. Data are vertically shifted for clarity by a factor of 10, 1, and 0.1, respectively. Corresponding model fits of a polydisperse cylinder form factor are also shown (black lines), and demonstrate a decrease in the rod diameter from (red) 290 nm, (green) 140 nm, and (blue) 90 nm. Inset SEM images also showed a decrease in diameter with excess PVP and citrate. Inset scale bar is 300 nm.

4. Conclusions

In summary, the combined effects of temperature, sonication, citrate precipitation, and emulsion composition were explored with the goals of controlling and reducing the dimensions of anisotropic silica colloids further into the nanoscale. A route to reduce anisotropic silica particle dimensions by at best five-fold ($D \approx 60$ nm, $L \approx 300$ nm) incorporated the addition of excess PVP and excess sodium citrate to the standard emulsion conditions. Combined addition of excess PVP and citrate was speculated to both drive down the emulsion droplet size while constraining citrate precipitation, thereby reducing the rod diameter relative to the standard conditions [3]. Alternatively, increasing temperature was shown to reduce particle diameters to at best $D \approx 150$ nm, in agreement with previous findings [14], but also generated curved, branched, and hollow-ended silica structures. Applying bath sonication during the reaction produced multimodal distributions of thin rods, long fibers, and standard rods, while adjusting bath sonication power and temperature did not improve control over the size distributions or production of smaller rods. Alternatively, it was shown that thin rods or fibers could be produced by addition of excess sodium citrate, without the need for sonication. Together, these findings suggested a competition between the terminal-droplet growth mechanism [3] and a templated growth mechanism following citrate precipitation [18-20, 22], in which the latter was hypothesized to contribute to termination of anisotropic growth, rod tapering and tailing effects, and increased length polydispersities. The competition of templated growth was confirmed by TEM, which showed hollow core-shell silica rod structures under conditions of excess PVP and citrate. The PVP molecular weight and concentration dependence also suggested a fundamental dependence on polymer entanglements, which are speculated to enhance the elasticity and steric stability of the terminal droplet during anisotropic growth. Broadening our fundamental understanding of the interplay between PVP, citrate, ammonium ions, and emulsion instabilities introduced by citrate precipitation will further

improve control of anisotropic silica particle dimensions, shape, yield, polydispersity, and end-effects, all of which are of interest for use in various particle-based technologies. Continuing to understand and improve this scalable, one-pot synthetic approach will provide shape-specific colloidal model systems to systematically explore the effects of particle size, shape anisotropy, and polydispersity on colloidal suspension rheology.

ASSOCIATED CONTENT

Supporting Information. The following files are available free of charge: List of reagents, (Table S1) Synthesis conditions and reagent additions, (Table S2) Particle sizing measurements from SEM, (Table S3) USAXS form factor model fit parameters, (Figure S1) Additional SEM images of side-effects from increasing reaction temperature, (Figure S2) Additional SEM images of excess citrate and silica fiber formation, (Figure S3) Additional TEM images of tapering and tailing effects, (Figure S4) Additional TEM images of hollow core-shell rods and end-effects, (Figure S5) Additional SEM images of PVP molecular weight dependence, (Figure S6) Additional SEM images of low MW PVP concentration dependence.

AUTHOR INFORMATION

Corresponding Author

*E-mail: wagnernj@udel.edu

Notes

The authors declare no competing financial interests.

ACKNOWLEDGMENT

The authors acknowledge financial support from the University of Delaware (UD) and the National Institute of Standards and Technology (NIST) under the cooperative agreements 70NANB10H256 and 70NANB12H239. Particle synthesis and imaging were conducted at the Center for Nanophase Materials Sciences (CNMS), which is a DOE Office of Science User Facility. This research used resources of the Advanced Photon Source, a U.S. Department of Energy (DOE) Office of Science User Facility operated for the DOE Office of Science by Argonne National Laboratory under Contract No. DE-AC02-06CH11357. X-ray scattering data was collected at the USAXS beamline 9-ID-C at the Advanced Photon Source, Argonne National Laboratory, with the assistance of Dr. Jan Ilavsky. The authors acknowledge the UD W. M. Keck Center for Advanced Microscopy and Microanalysis for use of TEM. This work benefitted from SasView software originally developed by the DANSE project under NSF award DMR-0520547. The authors also thank Michelle Pawel (CNMS) for her technical assistance.

REFERENCES

- [1] R.K. Iler, *The Chemistry of Silica: Solubility, Polymerization, Colloid and Surface Properties and Biochemistry of Silica*, Wiley-Interscience 1979.
- [2] J. Mewis, N.J. Wagner, *Colloidal suspension rheology*, Cambridge University Press, New York, 2012.
- [3] A. Kuijk, A. van Blaaderen, A. Imhof, Synthesis of Monodisperse, Rodlike Silica Colloids with Tunable Aspect Ratio, *J. Am. Chem. Soc.* 133(8) (2011) 2346-2349.
- [4] J. Zhang, H. Liu, Z. Wang, N. Ming, Au-induced polyvinylpyrrolidone aggregates with bound water for the highly shape-selective synthesis of silica nanostructures, *Chemistry* 14(14) (2008) 4374-80.
- [5] A. Kuijk, D.V. Byelov, A.V. Petukhov, A. van Blaaderen, A. Imhof, Phase behavior of colloidal silica rods, *Faraday Discuss.* 159 (2012) 181.
- [6] T. Xu, V.A. Davis, Liquid crystalline phase behavior of silica nanorods in dimethyl sulfoxide and water, *Langmuir* 30(16) (2014) 4806-13.
- [7] B. Liu, T.H. Besseling, M. Hermes, A.F. Demirors, A. Imhof, A. van Blaaderen, Switching plastic crystals of colloidal rods with electric fields, *Nat. Commun.* 5 (2014) 3092.
- [8] B. Liu, T.H. Besseling, A. van Blaaderen, A. Imhof, Confinement Induced Plastic Crystal-to-Crystal Transitions in Rodlike Particles with Long-Ranged Repulsion, *Phys. Rev. Lett.* 115(7) (2015) 078301.

- [9] R.P. Murphy, K. Hong, N.J. Wagner, Thermoreversible Gels Composed of Colloidal Silica Rods with Short-Range Attractions, *Langmuir* 32(33) (2016) 8424-35.
- [10] B.W. Longbottom, L.A. Rochford, R. Beanland, S.A. Bon, Mechanistic Insight into the Synthesis of Silica-Based "Matchstick" Colloids, *Langmuir* 31(33) (2015) 9017-25.
- [11] K. Chaudhary, Q. Chen, J.J. Juarez, S. Granick, J.A. Lewis, Janus colloidal matchsticks, *J. Am. Chem. Soc.* 134(31) (2012) 12901-3.
- [12] P. Datskos, J. Chen, J. Sharma, Addressable morphology control of silica structures by manipulating the reagent addition time, *RSC Adv.* 4(5) (2014) 2291-2294.
- [13] P. Datskos, D.A. Cullen, J. Sharma, Step-by-Step Growth of Complex Oxide Microstructures, *Angew. Chem. Int. Ed. Engl.* 54 (2015) 9011-9015.
- [14] P. Datskos, J. Sharma, Synthesis of segmented silica rods by regulation of the growth temperature, *Angew. Chem. Int. Ed. Engl.* 53(2) (2014) 451-4.
- [15] F. Hagemans, E.B. van der Wee, A. van Blaaderen, A. Imhof, Synthesis of Cone-Shaped Colloids from Rod-Like Silica Colloids with a Gradient in the Etching Rate, *Langmuir* 32(16) (2016) 3970-6.
- [16] B. Peng, G. Soligno, M. Kamp, B. de Nijs, J. de Graaf, M. Dijkstra, R. van Roij, A. van Blaaderen, A. Imhof, Site-specific growth of polymers on silica rods, *Soft Matter* 10(48) (2014) 9644-50.
- [17] A. Kuijk, A. Imhof, M.H.W. Verkuijlen, T.H. Besseling, E.R.H. van Eck, A. van Blaaderen, Colloidal Silica Rods: Material Properties and Fluorescent Labeling, *Part. Part. Syst. Charact.* 31(6) (2014) 706-713.
- [18] H. Nakamura, Y. Matsui, The Preparation of Novel Silica Gel Hollow Tubes, *Advanced Materials* 7(10) (1995) 871-872.
- [19] H. Nakamura, Y. Matsui, Silica Gel Nanotubes Obtained by the Sol-Gel Method, *J. Am. Chem. Soc.* 117 (1995) 2651-2652.
- [20] H. Nakamura, Y. Matsui, T. Goto, Fine silica tube and process for making same, US, 5573983, 1996.
- [21] J. Sharma, Finite-Sized One-Dimensional Silica Microstructures (Rods): Synthesis, Assembly, and Applications, *ChemNanoMat* (2017).
- [22] F. Miyaji, S.A. Davis, J.P.H. Charmant, S. Mann, Organic Crystal Templating of Hollow Silica Fibers, *Chem. Mater.* 11 (1999) 3021-3024.
- [23] W. Stober, A. Fink, E. Bohn, Controlled Growth of Monodisperse Silica Spheres in the Micron Size Range, *J Colloid Interface Sci* 26 (1968) 62-69.
- [24] P. Datskos, J. Chen, J. Sharma, Synthesis of very small diameter silica nanofibers using sound waves, *Chem. Commun.* 50(55) (2014) 7277-9.
- [25] J. Ilavsky, Nika: software for two-dimensional data reduction, *J. Appl. Crystallogr.* 45(2) (2012) 324-328.
- [26] J. Ilavsky, P.R. Jemian, Irena: tool suite for modeling and analysis of small-angle scattering, *J. Appl. Crystallogr.* 42(2) (2009) 347-353.
- [27] J. Ilavsky, P.R. Jemian, A.J. Allen, F. Zhang, L.E. Levine, G.G. Long, Ultra-small-angle X-ray scattering at the Advanced Photon Source, *J. Appl. Crystallogr.* 42(3) (2009) 469-479.
- [28] S.R. Kline, Reduction and analysis of SANS and USANS data using IGOR Pro, *J. Appl. Crystallogr.* 39(6) (2006) 895-900.
- [29] SasView, 2016. <http://www.sasview.org/>.

- [30] A.Q. Zhang, H.J. Li, D.J. Qian, M. Chen, Kinetically-controlled template-free synthesis of hollow silica micro-/nanostructures with unusual morphologies, *Nanotechnology* 25(13) (2014) 135608.
- [31] L. Wang, S. Tomura, F. Ohashi, M. Maeda, M. Suzuki, K. Inukai, Synthesis of single silica nanotubes in the presence of citric acid, *Journal of Materials Chemistry* 11(5) (2001) 1465-1468.
- [32] C. Graf, D.L.J. Vossen, A. Imhof, A. van Blaaderen, A General Method To Coat Colloidal Particles with Silica, *Langmuir* 19(17) (2003) 6693-6700.
- [33] E. Nemati-Kande, H. Shekaari, Liquid-Liquid Equilibria of Some Aliphatic Alcohols +Disodium Hydrogen Citrate +Water Ternary Systems at 298.15 K, *J Solution Chem* 41 (2012) 1649-1663.
- [34] M.T. Zafarani-Moattar, S. Banisaeid, M.A.S. Beirami, Phase Diagrams of Some Aliphatic Alcohols + Potassium or Sodium Citrate + Water at 25 °C, *J. Chem. Eng. Data* 50 (2005) 1409-1413.
- [35] S.L. Shenoy, W.D. Bates, H.L. Frisch, G.E. Wnek, Role of chain entanglements on fiber formation during electrospinning of polymer solutions: good solvent, non-specific polymer-polymer interaction limit, *Polymer* 46(10) (2005) 3372-3384.

TOC Figure

